# Off-plane motion of a prolate capsule in shear flow

C. DUPONT[1,2], A.-V. SALSAC[1]
AND D. BARTHÈS-BIESEL[1]

[1]Laboratoire de Biomécanique et Bioingénierie (UMR CNRS 7338), Université de Technologie de Compiègne, BP 20529, 60205 Compiègne, France

[2] Laboratoire de Mécanique des Solides (UMR CNRS 7649), Ecole Polytechnique, 91128 Palaiseau Cedex, France

(Received January 22, 2013)

The objective is to study the motion of an ellipsoidal capsule in a simple shear flow when its revolution axis is initially placed off the shear plane. We consider prolate capsules with an aspect ratio of 2 or 3 enclosed by a membrane, which is either strain-hardening or strain-softening. We seek the equilibrium motion of the capsule as we increase the capillary number $Ca$, which measures the ratio between the viscous and elastic forces. The three-dimensional fluid-structure interaction problem is solved numerically by coupling a boundary integral method (for the internal and external flows) with a finite element method (for the wall deformation). For any initial inclination with the flow vorticity axis, a given capsule converges towards a unique equilibrium configuration which depends on $Ca$. At low capillary number, the stable equilibrium motion is the *rolling* regime: the capsule aligns its long axis with the vorticity axis, while the membrane tank-treads entrained by the shear flow. As $Ca$ increases, the capsule takes a complex *wobbling* motion at equilibrium, precessing around the vorticity axis. As $Ca$ is further increased, the capsule long axis oscillates about the shear plane, while the membrane rotates around a capsule cross-section that also oscillates over time (*oscillating-swinging* regime). The amplitude of the oscillations about the shear plane decreases as $Ca$ increases and the capsule finally takes a *swinging* motion in the shear plane. It is found that the transitions from rolling to wobbling and from wobbling to oscillating-swinging depend on the mean energy stored in the membrane.

## 1. Introduction

Capsules are small liquid droplets enclosed by a thin deformable elastic membrane. They are used to protect and transport the particle internal content. Many occurrences may be found in nature (cells, eggs, seeds), but capsules have also numerous applications in bioengineering, pharmaceutics and cosmetics.

Nowadays artificial capsules can be produced in large quantities by first creating an emulsion and then adding a cross-linking agent to form a membrane around the droplets (Chang *et al.* 1966; Lévy *et al.* 1991, 1994, 1995; Edwards-Lévy *et al.* 1993, 1994; Andry *et al.* 1996). This results in the fabrication of capsules that are approximately spherical in shape. However, non-spherical capsules have a higher surface-to-volume ratio than spherical ones (for the same internal volume) and could therefore be interesting to use in order to enhance mass transfer between the internal and external media (Schneeweiss & Rehage 2005). Nature has taken this course with red blood cells, which are small biconcave disks. Microfluidic systems have been developed recently to produce non-spherical artificial capsules. In particular Liu *et al.* (2009) and Xiang *et al.* (2008) have fabricated oblate and prolate microcapsules with arbitrary aspect ratio. More recently, Koleva & Rehage (2012) have fabricated slightly oblate polysiloxane capsules with an aspect ratio of 0.97-0.99.

When an initially spherical capsule is suspended in a simple shear flow, it elongates in the straining direction, while the vorticity of the flow induces a *tank-treading* rotation of the membrane around a steady deformed shape (Barthès-Biesel & Rallison 1981; Ramanujan & Pozrikidis 1998; Lac *et al.* 2004; Li & Sarkar 2008). In the case of a slightly non-spherical capsule, Chang & Olbricht (1993) and Walter *et al.* (2001) have observed experimentally a more complex behaviour (the capsules used by Walter *et al.* have an aspect ratio of approximately 0.97). The capsule appears to have a *tank-treading* motion in the shear plane but undergoes small oscillations about the straining direction. This regime was also observed by Abkarian *et al.* (2007) for red blood cells and is now called *swinging*. As the shear rate increases, the swinging regime evolves towards a tank-treading regime where the cell orientation is steady. At low shear rates, red blood cells have a solid-like *tumbling* motion, where they rotate as a solid body about the vorticity axis (Abkarian & Viallat 2008). Furthermore, Dupire *et al.* (2012) observed that the orbit of the red blood cell is unstable near the transition between the tumbling and the swinging regimes. Such an intermittent regime was also observed by Koleva & Rehage (2012).

Motivated by the experimental observations on red blood cells, numerical simulations have been carried out to understand the behaviour of non-spherical capsules in shear flow (Ramanujan & Pozrikidis 1998; Sui *et al.* 2008; Walter *et al.* 2011). These studies have considered the motion of an oblate capsule in a simple shear flow, in view of their relevance to red blood cells. Only Walter *et al.* (2011) have additionally studied the behaviour of a prolate capsule. In all these numerical studies, the revolution axis of the capsule is initially positioned in the shear plane. Since the fluid inertia is either neglected or very small, Stokes flow conditions prevail and by symmetry the capsule axis must remain in the shear plane where it reaches an equilibrium periodic motion. These numerical models show that at low shear rate, the capsule rotates ('tumbles') about the vorticity axis as a quasi-solid body. As the shear rate increases, the capsule elongates in the maximum strain rate direction and the membrane rotates. However, since the initial geometry is not isotropic, the capsule elongation and orientation oscillate about mean values as observed experimentally in the swinging regime. The behaviour of prolate and oblate capsules is qualitatively the same, but the transition between tumbling and swinging occurs at lower shear rates for the oblate capsules (Walter *et al.* 2011).

For spheroidal capsules, there is another obvious equilibrium configuration, which occurs when the capsule revolution axis is perpendicular to the shear plane. From symmetry considerations, it is clear that in Stokes flow, the capsule axis must then remain parallel to the vorticity axis. The sections of the capsule parallel to the shear plane lose their initial circular shape and are elongated in the strain direction, while the membrane tank-treads about the steady deformed shape. We will call this motion mode *rolling*, with reference to Abkarian *et al.* (2001) and Dupire *et al.* (2012). Of course in experiments, the capsule revolution axis is rarely aligned with either the shear flow or the vorticity axis. This raises the question of the *mechanical stability* of the motion of a capsule initially positioned with its axis in the shear plane or perpendicular to it.

The objective of this paper is thus to study the motion of a capsule in a simple shear flow when its revolution axis is initially positioned *off* the shear plane. We will consider prolate capsules and thus complement the work of Walter *et al.* (2011). The advantage of working with this geometry is that the tumbling-to-swinging transition occurs at higher shear rates for prolate than for oblate capsules, which facilitates the computations. In particular we will demonstrate that the capsule typically deviates from the tumbling and swinging motions, when the revolution axis is initially placed outside the shear plane.

The motion of a capsule in a flow is a classical fluid-structure interaction problem. We use the numerical method developed by Walter *et al.* (2010) to treat this problem. This method, based on the coupling of a membrane finite element method for the capsule deformation with a boundary integral method for the internal and external flows, has been shown to be very precise and to remain numerically stable. The problem and the numerical method are briefly outlined in § 2. The behaviour of a prolate capsule initially positioned off the shear plane is presented in § 3 as a function of the shear rate. The effect of membrane law and aspect ratio on the capsule motion is shown in § 4. The results are then discussed in § 5.

## 2. Problem statement and numerical method

### 2.1. *Problem statement*

We consider an initially spheroidal capsule and denote $2a$ the length of the revolution axis and $2b$ the length of the two orthogonal axes. The capsule is prolate with aspect ratio $a/b$. We define a length scale $\ell = (ab^2)^{1/3}$ as the radius of the sphere with the same volume as the capsule. We shall consider two capsule shapes corresponding to $a/b = 2$ $(a/\ell = 1.587, b/\ell = 0.794)$ and $a/b = 3$ $(a/\ell = 2.08, b/\ell = 0.693)$ respectively. The reference frame based on the undeformed capsule principal axes is denoted $\mathcal{R}'$ (O, $\mathbf{e'}_x$, $\mathbf{e'}_y$, $\mathbf{e'}_z$), where O is the centre of mass of the capsule. Assuming that the revolution axis is along $\mathbf{e'}_z$, the capsule surface is given by

$$\left(\frac{x'}{b}\right)^2 + \left(\frac{y'}{b}\right)^2 + \left(\frac{z'}{a}\right)^2 = 1, \tag{2.1}$$

where $(x', y', z')$ is the position of a membrane material point.

The capsule is filled with a Newtonian incompressible fluid with viscosity $\mu$. It is freely suspended in an unbounded Newtonian incompressible fluid with the same viscosity $\mu$. The external fluid is subjected to a simple shear flow with shear rate $\dot{\gamma}$ and undisturbed velocity

$$\mathbf{v}^\infty = \dot{\gamma} y \mathbf{e}_x \tag{2.2}$$

in the laboratory reference frame $\mathcal{R}$ $(\mathrm{O}, \mathbf{e}_x, \mathbf{e}_y, \mathbf{e}_z)$. The Reynolds number of the flow is assumed to be very small. Thus, the internal and external flows are governed by the Stokes equations. The symmetry of the problem and of the governing equations implies that, when the revolution axis of a capsule is initially in the shear plane or perpendicular to it, it remains as such.

At time $\dot{\gamma}t = 0$, the position of the capsule in space is defined by the angles between the basis vectors of frames $\mathcal{R}'$ and $\mathcal{R}$. As shown in Figure 1, we chose $(\mathbf{e}_x, \mathbf{e'}_x) = 0$ and $(\mathbf{e}_z, \mathbf{e'}_z) = (\mathbf{e}_y, \mathbf{e'}_y) = \zeta_0$. This means that the capsule revolution axis initially makes an angle $\zeta_0$ with the vorticity axis and an angle $\pi/2 - \zeta_0$ with the shear plane.

The capsule membrane is modeled as an isotropic hyperelastic surface with shear modulus $G_s$ and area dilatation modulus $K_s$. Two types of membrane constitutive laws can be considered, where the material is either strain-softening or hardening (Barthès-Biesel *et al.* 2002). A strain-softening membrane can be described by the neo-Hookean law (NH). The principal elastic tensions $\tau_1$ and $\tau_2$ are then given in terms of the in-plane principal stretch ratios $\lambda_1$ and $\lambda_2$ by

$$\tau_1 = \frac{G_s}{\lambda_1 \lambda_2}\left[\lambda_1^2 - \frac{1}{(\lambda_1 \lambda_2)^2}\right] \qquad \text{(likewise for } \tau_2\text{)}. \tag{2.3}$$

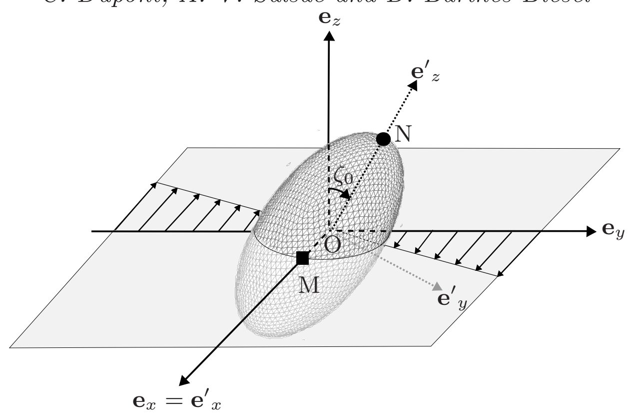


Figure 1: Reference configuration of the prolate capsule at $\dot{\gamma}t = 0$. The capsule inclination $\zeta_0$ is the initial angle between the flow vorticity axis $\mathbf{e}_z$ and the capsule revolution axis $\mathbf{e}'_z$. During the capsule deformation, we will follow the motion of two specific points of the capsule membrane: the point M is initially on the short axis $\mathbf{e}'_x$ (■) and the point N on the long axis $\mathbf{e}'_z$ (●).

The surface shear and area dilatation moduli are related by $K_s/G_s = 3$. Conversely, a strain-hardening membrane can be described by the Skalak law (SK), initially proposed by Skalak *et al.* (1973) to model the red blood cell membrane

$$\tau_1 = \frac{G_s}{\lambda_1\lambda_2}\left[\lambda_1^2(\lambda_1^2-1) + C(\lambda_1\lambda_2)^2\left((\lambda_1\lambda_2)^2-1\right)\right] \qquad \text{(likewise for } \tau_2\text{)}. \tag{2.4}$$

The surface shear and area dilatation moduli are then related by $K_s = G_s(1+2C)$, where $C$ is a constant such that $C > -1/2$. For $C = 1$ ($K_s/G_s = 3$), the two laws NH and SK lead to the same small deformation behavior. Note that the Skalak membrane material can undergo surface area-changes while being strain-hardening.

The capsule motion and deformation are thus governed by the membrane constitutive law, the ratio of the area dilatation and shear moduli $K_s/G_s$, the particle initial aspect ratio $a/b$ and initial orientation $\zeta_0$, and by the capillary number $Ca = \mu\dot{\gamma}\ell/G_s$, which measures the ratio between the viscous and the elastic forces.

### 2.2. *Numerical method*

The motion and deformation of the capsule are solved by means of the numerical technique developed by Walter *et al.* (2010). This method couples a membrane finite element method (for the mechanics of the capsule wall) with a boundary integral method (for the internal and external flows). The method is briefly described in this subsection. More details on the procedure may be found in Walter *et al.* (2010) or in the book chapter (Barthès-Biesel *et al.* 2010).

At time $\dot{\gamma}t = 0$, the capsule is in its reference ellipsoidal shape, when we start the flow. We then perform a Lagrangian tracking of the position of the membrane material points over time. At a given time, the position of the material points is known and we may thus compute the stretch ratios $\lambda_1$ and $\lambda_2$ and the elastic tension tensor $\boldsymbol{\tau}$ from equation (2.4). The load $\mathbf{q}$ exerted by the fluids on the membrane is found by using the finite element method to solve the membrane equilibrium equation

$$\boldsymbol{\nabla}_s \cdot \boldsymbol{\tau} + \mathbf{q} = 0, \tag{2.5}$$

where $\boldsymbol{\nabla}_s$ represents a surface gradient. The fluid velocity may be written as a boundary integral on the deformed surface $S$ of the capsule

$$\mathbf{v}(\mathbf{x}) = \mathbf{v}^{\infty}(\mathbf{x}) - \frac{1}{8\pi\mu}\int_S \left(\frac{\mathbf{I}}{\parallel \mathbf{r} \parallel} + \frac{\mathbf{r}\otimes\mathbf{r}}{\parallel \mathbf{r} \parallel^3}\right)\cdot \mathbf{q}(\mathbf{y}) dS(\mathbf{y}), \tag{2.6}$$

where $\mathbf{v}(\mathbf{x})$ is the velocity of the membrane point located at $\mathbf{x}$, $\mathbf{r} = \mathbf{x} - \mathbf{y}$ and $\mathbf{I}$ is the identity tensor. An explicit second-order Runge-Kutta method is then used to integrate the velocity and obtain the new position of the membrane points at the following time step.

### 2.3. *Discretization, stability and convergence*

The surface of the capsule is discretized with triangular curved $P_2$ elements (Figure 1). The mesh is initially generated for a spherical capsule by inscribing an icosahedron (regular polyhedron with 20 triangular faces) in a sphere. The elements are subdivided sequentially until the desired number of elements is reached (Ramanujan & Pozrikidis 1998; Walter *et al.* 2010). At the last step, nodes are added at the middle of all the element edges and projected onto the sphere in order to generate the $P_2$ elements. The mesh is then deformed into an ellipsoid following equation 2.1. In the study, the capsule mesh has 2562 nodes and 1280 elements.

The numerical method is stable, when the time step satisfies the condition $\dot{\gamma} \triangle t < O(hCa)$, where $h$ is the typical non-dimensional mesh size (Walter *et al.* 2010). We use $\dot{\gamma} \triangle t = 5 \times 10^{-3}$ for $Ca \geqslant 0.5$ and decrease the time step proportionally for lower $Ca$.

A capsule initially placed off the shear plane takes a very long time to reach the equilibrium state. Computational times of the order of $\dot{\gamma}t = 10^2 - 10^3$ are therefore needed to capture the dynamics. With such long computational times, the numerical error may no longer be negligible. We thus monitor the relative error $\varepsilon_V = |V - V_0|/V_0$ on the capsule volume $V$, where $V_0$ is the capsule initial volume. For off-plane capsules, the error at $\dot{\gamma}t = 100$ is $\sim \mathcal{O}(10^{-2})$ for $Ca \leqslant 0.9$ and $\mathcal{O}(10^{-3})$ for $Ca > 0.9$.

### 2.4. *Result analysis*

Depending on the parameters, the capsule motion and deformation become complex and difficult to analyze. The global geometry of the capsule is evaluated by means of the ellipsoid of inertia of the deformed shape. We denote $L_i$ the half lengths of the principal axes of the ellipsoid of inertia ($L_1 > L_2 > L_3$) and $\mathbf{v}_i$ the corresponding unit vectors in $\mathcal{R}$ ($\mathbf{v}_1 = \mathbf{e}'_z$ at time $\dot{\gamma}t = 0$ for a prolate capsule). The membrane rotation is measured from the motion of two points (Figure 1):

- the point M is the Lagrangian position at time $\dot{\gamma}t$ of the membrane point that was initially located on the capsule short axis $\mathbf{e}'_x$.
- the point N is the Lagrangian position at time $\dot{\gamma}t$ of the membrane point that was initially located on the capsule long axis $\mathbf{e}'_z$.

The capsule global motion is measured from the position of the capsule tip P, which corresponds to the Eulerian position in $\mathcal{R}$ of the intersection between the $\mathbf{v}_1$ axis and the membrane. At time $\dot{\gamma}t = 0$, the points N and P are superimposed. The projections of P in the shear $xy-$plane or in the $xz-$plane are denoted P' and P", respectively.

The capsule deformation can be analyzed using the Taylor parameters

$$D_{ij} = \frac{L_i - L_j}{L_i + L_j} \quad (i, j = 1, 2, 3 \text{ and } i \neq j). \tag{2.7}$$

Owing to the capsule initial ellipsoidal shape, the initial values of the Taylor parameters are $D^0_{23} = 0$ and $D^0_{12} = D^0_{13} = (a - b)/(a + b) = 1/3$ for an aspect ratio $a/b = 2$ or 1/2 for $a/b = 3$. The overall deformation can also be measured by the elastic energy $E$ stored

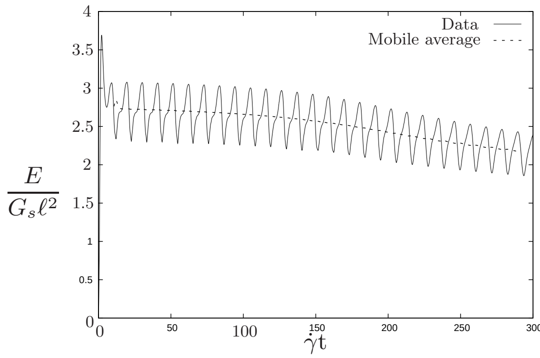


Figure 2: Time evolution of the elastic energy $E/G_s\ell^2$ stored in the membrane (solid line) for a C2SK capsule with $\zeta_0 = 85^\circ$ and $Ca = 0.9$. The mobile average (dotted line) is obtained with a non-dimensional period $\dot{\gamma}T = 21.55$.

in the capsule wall (Walter *et al.* 2010)

$$E(t) = \int_{S_0} w_s(\lambda_1, \lambda_2, t) dS_0, \tag{2.8}$$

where $w_s$ is the strain energy function per unit area of undeformed membrane and $S_0$ is the initial surface of the capsule.

In most cases, the capsule has a kind of gyroscopic motion, where it rotates and reorients itself. Correspondingly, the coordinates of any point, the membrane energy, the capsule deformation, etc. all have pseudo-periodic oscillations with amplitude changing over time. We have used a centred moving average method (Hay & Bull 2009) to smooth the data and to visualize the time evolution of the parameters (Figure 2). This method replaces a value $x(t)$ by its average over a period $T$ centred around the time value $t$. Here, we define the period of the motion as the time required for a point initially at $(x, 0, 0)$ to return on the $\mathbf{e}_x$ axis. Unless otherwise mentioned, all results pertain to quantities that are averaged over one period.

To simplify notations, we call C2SK and C3SK the capsules with a SK membrane of aspect ratios 2 and 3, respectively, and C2NH the capsules with a NH membrane of aspect ratio 2.

## 3. Results

We first consider a prolate capsule $a/b = 2$ enclosed by a SK ($C = 1$) membrane, and study in detail the effect of the initial orientation $\zeta_0$ and of the flow strength measured by $Ca$. The influence of the membrane law and of the aspect ratio will be briefly discussed in section 4.

### 3.1. *Motion of a capsule with* $\zeta_0 = 90^\circ$

Before studying the motion of a capsule initially placed off the shear plane with an arbitrary angle, we will first summarize the dynamics of a capsule when its revolution axis is initially positioned in the shear plane ($\zeta_0 = 90^\circ$). Walter *et al.* (2011) have shown that the long axis remains in the shear plane. They have also shown that the capsule motion is a function of the capillary number $Ca$. At low capillary numbers ($Ca < 0.25$), the capsule rotates about the vorticity axis like a quasi-solid particle; its cross-section

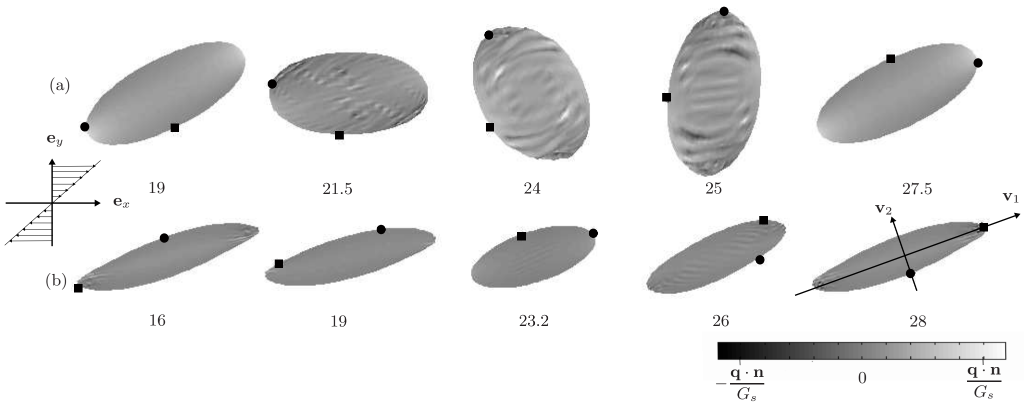


Figure 3: Capsule C2SK shape when $\zeta_0 = 90^\circ$: shape evolution over one half period at steady state for $Ca = 0.1$ (a) and $Ca = 2$ (b). The grey scale corresponds to the normal component of the load $\mathbf{q} \cdot \mathbf{n}$ on the membrane. The maximum values of the normal load are $\mathbf{q} \cdot \mathbf{n}/G_s = 0.9$ (a) and 25 (b). The value of the non-dimensional time $\dot{\gamma}t$ is given below each shape. The points M (■) and N (●) were initially on the short and long axis respectively (Figure 1).

with the shear plane exhibits small deformations (Figure 3a). This regime is referred to as *tumbling*.

For $Ca > 0.35$, the capsule has a quasi-fluid behaviour. The angle of the capsule long axis with the streamlines and the capsule deformation oscillate about mean values (Figure 3b), because of the geometrical anisotropy of the initial shape. This is the so-called *swinging* regime. As $Ca$ increases, the membrane deformation increases and the long axis is tilted towards the streamlines. Furthermore, the oscillation amplitudes of the deformation and orientation also decrease with increasing $Ca$. Asymptotically, the capsule tends towards the pure tank-treading regime, where the membrane rotates around a steady deformed profile.

### 3.2. *Motion of a capsule with* $\zeta_0 = 0^\circ$

There is no available study of the case where the revolution axis of the capsule is initially perpendicular to the shear plane and thus parallel to the vorticity axis ($\zeta_0 = 0^\circ$). In this situation, the capsule long axis remains parallel to the vorticity for symmetry reasons. The shear flow exerts a viscous torque on the membrane and thus the capsule cross-sections parallel to the shear plane that were initially circular become elongated in the strain direction. The membrane then rotates around the steady capsule shape as shown in Figure 4. This capsule motion is the same for all the values of the capillary number and is called the *rolling* regime.

In order to further investigate the evolution of the capsule deformation, we have plotted the Taylor parameters calculated at steady state in Figure 5a. For low flow strength the principal direction $\mathbf{v}_1$ is along the vorticity axis. The deformation within the shear plane is thus measured by $D_{23}$, which sharply increases from zero (initially circular cross-section) to a plateau value a little above 0.5 (of the same order as the maximum deformation for a spherical capsule in simple shear flow). The deformation in planes perpendicular to the shear plane are measured by $D_{12}$ and $D_{13}$. The decrease of $D_{12}$ with $Ca$ is due to the pinching of the capsule by the straining effect of the shear flow. For $Ca \geqslant 1.5$, the capsule reaches a shape that is hardly influenced by the flow strength.

The maximum value $\tau_{max}$ of the principal elastic tensions within the membrane is

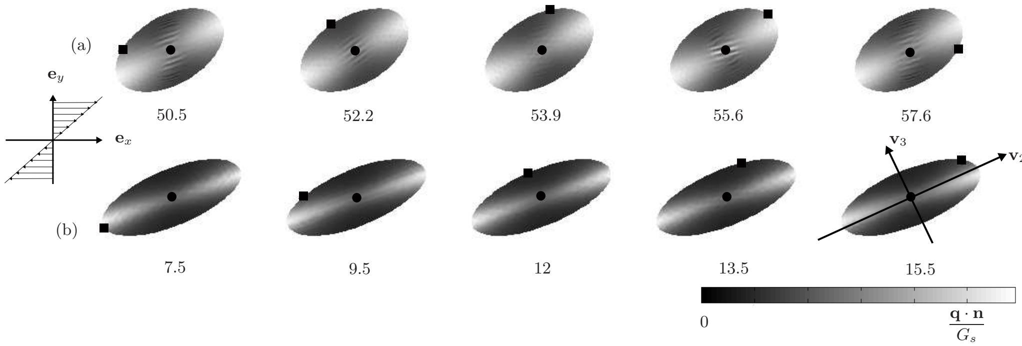


Figure 4: Capsule C2SK shape when $\zeta_0 = 0°$: shape evolution over one half period at steady state for $Ca = 0.1$ (a) and $Ca = 0.6$ (b). Same legend as in figure 3. The maximum values of the normal load are $\mathbf{q} \cdot \mathbf{n}/G_s = 0.5$ (a) and 2.5 (b).

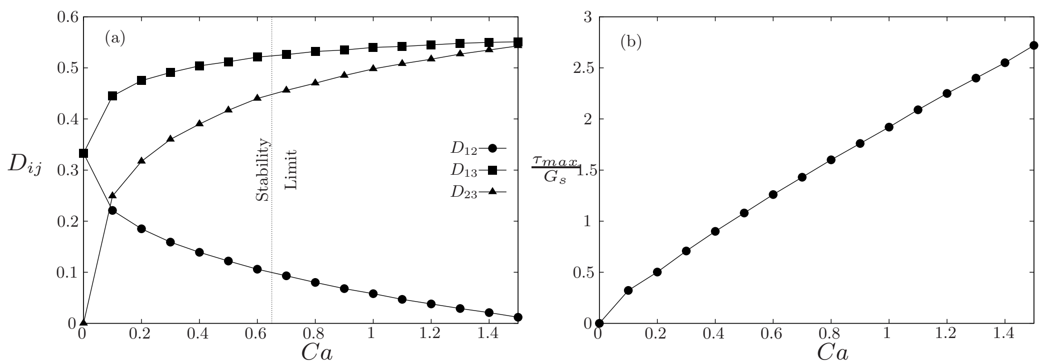


Figure 5: Capsule C2SK: influence of the capillary number $Ca$ on the rolling regime at $\zeta_0 = 0°$. (a) Capsule deformation estimated by the Taylor parameters $D_{ij}$, where the dotted line represents the stability limit; (b) maximum membrane tension $\tau_{max}$.

shown in Figure 5b. We find that the elastic tension level and correlatively the risk of rupture increase quasi-linearly with $Ca$. The maximum is located in the shear plane at the capsule edge in the $\mathbf{v}_3$ principal direction (see Figure 4). This is where the rupture will most likely occur when the failure criterion of the membrane material is exceeded. The minimum of the principal tensions $\tau_{min}$ is found to be about zero for all the values of $Ca$ (data not shown). It is slightly negative until $Ca = 0.4$ ($\tau_{min}/G_s \in [-0.04, 0]$), so that the membrane undergoes moderate compression locally. This explains why wrinkles appear at the capsule apices along the long axis (i.e. $\mathbf{v}_1$) in Figure 4 for $Ca = 0.1$ and not for $Ca = 0.6$.

Although we have shown results for large values of $Ca$, we will see in the following that for $Ca > 0.6$, the rolling configuration is no longer mechanically stable.

### 3.3. *Off-plane capsule at low flow strength ($Ca \leqslant 0.6$)*

When the capsule axis is displaced from the shear plane by a small angle of 5° ($\zeta_0 = 85°$), the capsule long axis does not go back to the shear plane (see supplementary movie file Movie 1). As shown in Figure 6a for $Ca = 0.1$, the projection P' of the capsule tip in the shear plane moves away from the fixed trajectory reached for $\zeta_0 = 90°$. It spirals around the flow vorticity axis $\mathbf{e}_z$ and eventually converges towards it. This is also apparent from

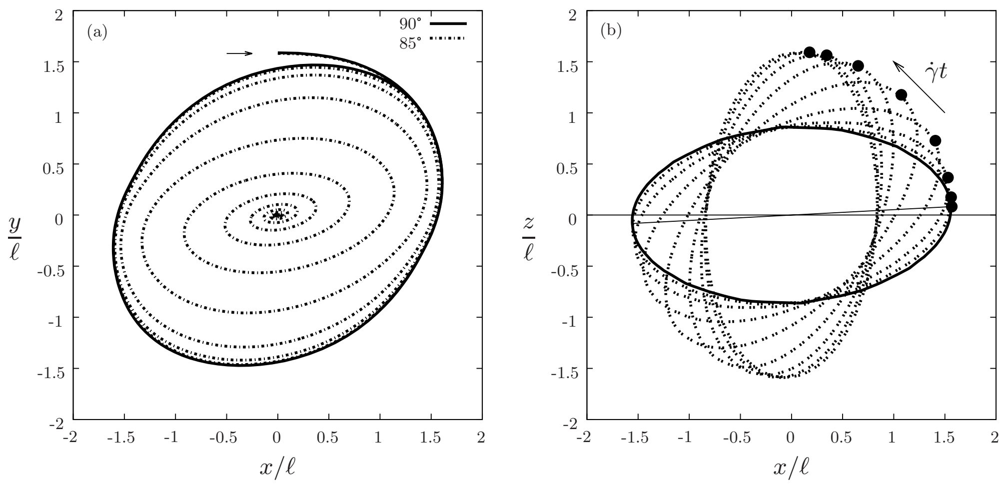


Figure 6: Motion of a C2SK capsule with $\zeta_0 = 85°$ at $Ca = 0.1$: (a) Comparison of the trajectory of point P' in the shear $xy-$plane with the case $\zeta_0 = 90°$. The arrow indicates the initial position of P'. (b) Evolution of the capsule shape in the $xz$-plane at the beginning of each period (solid line: capsule shape at $\dot{\gamma}t = 0$). The black point indicates the position of point P" at $\dot{\gamma}t = 5$, 22, 38, 55, 721, 89, 106, 123.

Figure 6b, which shows the evolution of the projection P" of point P in the $xz-$plane. The stable equilibrium position is thus the rolling regime. It is the converging position for any off-plane orientation $\zeta_0 < 90°$ (not shown). At equilibrium the capsule deformation and tank-treading motion are identical to those of the same capsule initially positioned at $\zeta_0 = 0°$ (Figures 4 and 5), i.e. with its revolution axis initially along the vorticity axis.

As shown in Figure 7, when the capsule is not constrained in the shear plane by symmetry, the elastic energy stored in the membrane decreases during the transient motion until it reaches the value for a rolling capsule. The equilibrium configuration is thus the one for which the mean deformation (as measured by the energy) is the smallest. We also note in Figure 7 that the initial orientation angle $\zeta_0$ influences the time the capsule needs to reach its equilibrium position. Indeed, the smaller the initial angle $\zeta_0$, the smaller the time. The transient time until equilibrium also increases with the capillary number (not shown).

In conclusion we find that, for $Ca$ up to 0.6, the *mechanically stable* situation corresponds to the *rolling* regime, a configuration where the capsule long axis is normal to the shear plane and the membrane tank-treads around it. Since the deformation is small at low capillary number, the capsule behaves almost as a solid ellipsoid and takes the position that dissipates the less energy (Jeffery 1922). Consequently, the tumbling motion found when the capsule axis is in the shear plane ($\zeta_0 = 90°$) is an *unstable* equilibrium state. Over long times, the accumulation of numerical errors is enough to slowly destabilize it. Considering the fact that in a suspension, the initial capsule orientation is usually random, we can expect that most of the capsules align their long axis with the flow vorticity and are eventually all in the rolling regime.

### 3.4. *Transition at moderate flow strength (*$0.6 < Ca < 1$*)*

For $Ca \geqslant 0.7$, the capsule no longer tends towards the rolling motion observed for lower values of $Ca$. Its motion is now a function of $Ca$.

For example, for $Ca = 0.9$ and different initial orientations $\zeta_0 \in ]0°, 90°[$, the time

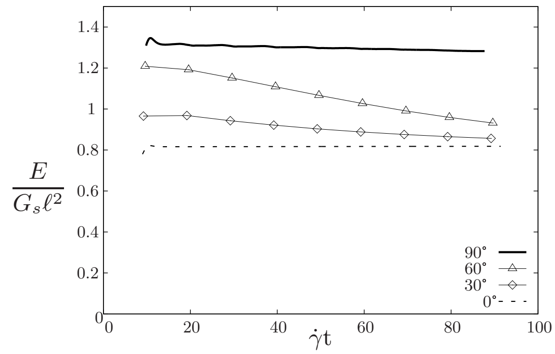


Figure 7: Capsule C2SK: time evolution of the elastic energy stored in the membrane $E/G_s\ell^2$, for various initial inclinations of the capsule with the shear plane ($Ca = 0.5$). The case $\zeta_0 = 90°$ represents the mechanically unstable tumbling motion.

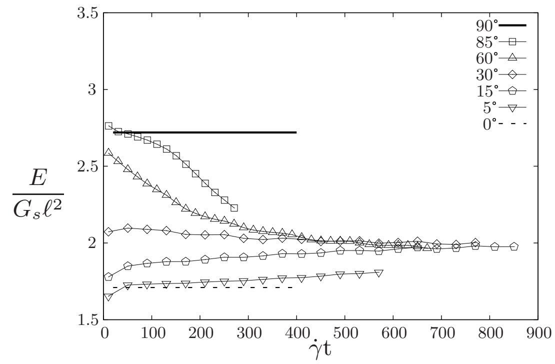


Figure 8: Capsule C2SK at $Ca = 0.9$: effect of the initial orientation on the time evolution of the elastic energy stored in the membrane $E/G_s\ell^2$

evolution of the mean elastic membrane energy $E/G_s\ell^2$ shows that it converges towards a common equilibrium value (Figure 8). For $Ca = 0.9$, this equilibrium state corresponds more or less to the motion that the capsule takes almost immediately (i.e. after a short transient) for an initial angle $\zeta_0 = 15 - 30°$.

We choose, therefore, to examine in detail the motion of a capsule with $\zeta_0 = 15°$ for $Ca = 0.9$ (see supplementary movie file Movie 2). The capsule rotates as a whole around the vorticity axis, while its tip P has a *wobbling* motion as shown in Figure 9. Indeed, the projection P' of P in the shear plane follows a roughly elliptical trajectory (Figure 9a), while the height of P above the shear plane oscillates (Figure 9b). This is of course different from the swinging motion obtained for $\zeta_0 = 90°$, where the tip of the capsule oscillates in the shear plane as shown in Figure 9a. We quantify this motion by means of $\zeta_{max}$, which corresponds to the maximum angle between the capsule longest principal axis $\mathbf{v}_1$ and the vorticity axis (in Figure 9b, one can see the projection of the angle $\zeta_{max}$ in the $xz-$plane). The value of $\zeta_{max}$ depends on $Ca$ as shown in Figure 10a. We retrieve the fact that for $Ca \leqslant 0.6$, $\zeta_{max} = 0°$, which corresponds to the rolling motion. As the capillary number is increased above 0.6, the capsule starts to precess around the vorticity axis with a maximum amplitude $\zeta_{max}$, which increases sharply with $Ca$.

The evolution of the mean elastic energy stored in the membrane at equilibrium $E^\infty$ (Figure 10b) also indicates clearly that the capsule bifurcates from the rolling regime

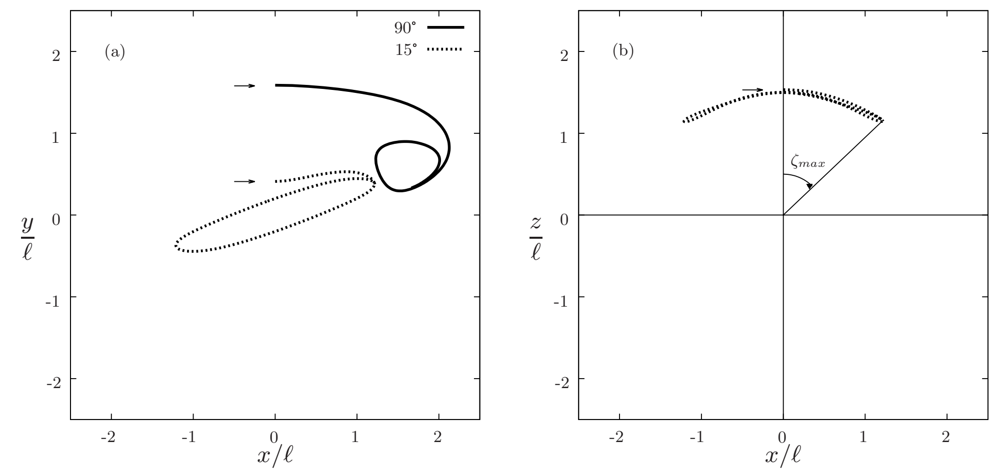


Figure 9: Motion of a C2SK capsule with $\zeta_0 = 15°$ at $Ca = 0.9$ up to the end of the first pseudo-period ($0 < \dot{\gamma}t < 26$): (a) trajectory of point P' in the shear plane (comparison with $\zeta_0 = 90°$); (b) trajectory of point P" in the $xz-$plane for $\zeta_0 = 15°$. The arrows indicate the initial position at $\dot{\gamma}t = 0$. The horizontal line at $z = 0$ represents the shear plane.

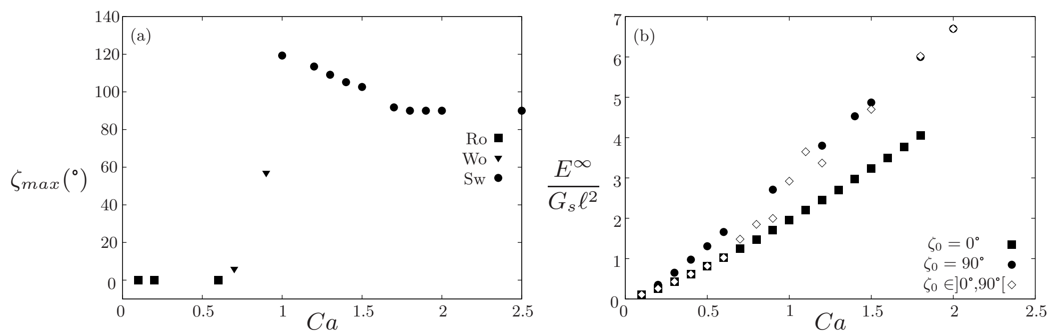


Figure 10: C2SK capsule. a) Evolution of the maximum inclination $\zeta_{max}$ of the capsule longest axis with the vorticity axis at equilibrium as a function of $Ca$: Ro: rolling, Wo: wobbling, Sw: oscillating-swinging tending to pure swinging. b) Evolution of the mean elastic energy $E^\infty$ stored in the membrane at equilibrium as a function of $Ca$ for initially off-plane capsules (diamond). Comparison with the cases $\zeta_0 = 0°$ (square) and 90° (circle).

($\zeta_0 = 0°$ curve) for $Ca \geqslant 0.7$. In the wobbling regime, the capsule deformation is still moderate but the energy of deformation is a little larger than the one that would be found in the rolling regime for the same $Ca$.

### 3.5. *Off-plane motion at high flow strength ($Ca \geqslant 1$)*

For a capillary number larger than 1, we find another type of motion. For example, for $Ca = 1.5$ and different initial orientations, the mean elastic membrane energy $E/G_s\ell^2$ converges in time towards a common value as shown in Figure 11. This equilibrium state is reached after a short transient for an initial angle $\zeta_0 = 60°$. The details of the motion of a capsule with $\zeta_0 = 60°$ at $Ca = 1.5$ are then shown in Figure 12 (see supplementary movie file Movie 3). The capsule assumes what we call an *oscillating-swinging* motion,

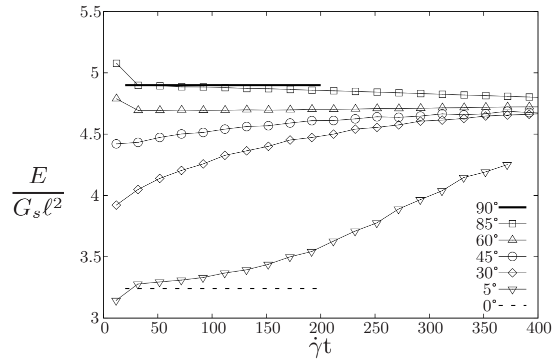


Figure 11: C2SK capsule at $Ca = 1.5$, effect of the initial orientation on the time evolution of the elastic energy stored in the membrane $E/G_s\ell^2$.

where the tip of the capsule oscillates both about the shear plane (Figure 12b) and within the shear plane about a mean inclination with respect to the flow direction (Figure 12a). The rotational motion is now taken over by the membrane as is apparent from the trajectory of point N in the shear plane (Figure 12a). This behavior corresponds to values of $\zeta_{max} \geqslant 90°$, as shown in Figure 10a.

As $Ca$ increases, the amplitude of the oscillations about the shear plane decreases. For large values of the capillary number $Ca \geqslant 1.8$, the capsule positions its long axis in the shear plane ($\zeta_{max} = 90°$) for any initial orientation $\zeta_0$: it undergoes the swinging regime described by Walter *et al.* (2011) and summarized in section 3.1. The convergence of the oscillating-swinging regime towards a pure swinging regime is also shown in Figure 10b: as $Ca$ increases, the equilibrium elastic energy tends towards the values obtained in the swinging regime. The evolution of the capsule profile at equilibrium is therefore similar to the one shown in Figure 3b for $\zeta_0 = 90°$. The membrane tank-treads around the time-oscillating profile. But, even these oscillations decrease as $Ca$ is increased: the capsule tends asymptotically towards a pure tank-treading motion at very large values of the capillary number. Correspondingly, the deformation energy tends towards the value obtained for the swinging regime as shown in Figure 10b.

### 3.6. *Global effect of Ca*

In conclusion, the motion and deformation of a prolate ellipsoidal capsule in shear flow depend in a complex way on the flow strength. There are two obvious equilibrium states for which the capsule keeps symmetry properties with respect to the shear plane and which correspond respectively to $\zeta_0 = 0$ or $90°$. The mean equilibrium energy stored in the membrane $E^\infty$ shown in Figure 10b indicates that the energy is larger when the capsule axis is in the shear plane ($\zeta_0 = 90°$) than when it is perpendicular to it ($\zeta_0 = 0°$). However, the energy criterion is not enough to govern the equilibrium state of the capsule even in Stokes flow. Indeed the capsule motion is the result of non-linear fluid–structure interactions. This may explain why there is a bifurcation from the rolling state towards the swinging state. During this transition, the capsule has first a quasi solid wobbling motion followed by a quasi fluid oscillating-swinging motion.

The question of the uniqueness of the equilibrium state then arises. In other words, is there an hysteresis effect? In order to give an answer to this question, we did the following experiment: starting from the oscillating-swinging equilibrium state found for $Ca = 1.5$, we have suddenly reduced the capillary number to $Ca = 0.9$. The resulting trajectory of the projection P" of the capsule tip in the $xz-$plane is shown in Figure 13. We note that

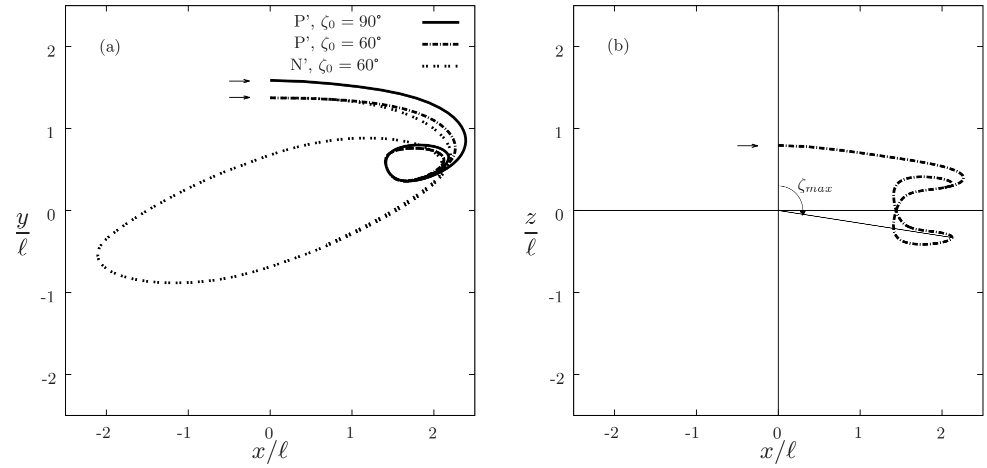


Figure 12: Motion of a C2SK capsule with $\zeta_0 = 60°$ at $Ca = 1.5$ up to the end of the first pseudo-period ($0 < \dot{\gamma}t < 29$): (a) trajectories of point P' (comparison with $\zeta_0 = 90°$) and of point N', the projection of point N in the shear plane; (b) trajectory of point P" in the $xz-$plane. The arrows indicate the initial position at $\dot{\gamma}t = 0$. The horizontal line at $z = 0$ represents the shear plane.

the amplitude of the oscillations of the capsule about the shear plane ($x-$axis) increases with time until the capsule switches to the wobbling motion. It converges towards the same configuration as obtained for a capsule initially at $Ca = 0.9$ as shown in Figure 9b. If then we suddenly decrease $Ca$ from 0.9 to 0.1, the capsule goes to the rolling regime described in section 3.3 (not shown). We thus conclude that the equilibrium states we find are unique.

## 4. Effect of membrane law and capsule aspect ratio

In order to assess the robustness of the results obtained with a SK law, we now consider a capsule with aspect ratio $a/b = 2$ and a strain-softening NH membrane. We find again that for low flow strength ($Ca \leqslant 0.5$), the stable mode of motion of the C2NH capsule is the rolling motion. In this regime, a capsule with a NH membrane is easier to deform than one with a SK membrane (Figure 14). Indeed for the same value of $Ca$, the capsule deformation is larger for a NH membrane than for a SK one.

As shown in Figure 15, for $Ca = 0.6$, the C2NH capsule has a wobbling motion followed by an oscillating-swinging motion for $Ca \geqslant 0.7$. However, for $Ca \geqslant 0.9$, the capsule does not seem to reach a steady trajectory. This is in agreement with the fact that there is no stable swinging regime in the shear plane for large values $Ca \geqslant 1$. Indeed, there is a critical flow strength for which the strain-softening elastic tension cannot balance the large viscous tension applied by the fluid (Barthès-Biesel 2011).

The case of a capsule with a SK membrane and aspect ratio $a/b = 3$ is now considered. Note that since we consider equal volume capsules, the capsule dimensions are now $a/\ell = 2.08$ and $b/\ell = 0.693$. The capsule cross-section is thus smaller than it is for $a/b = 2$. The rolling motion is again found to be the stable regime for $Ca \leqslant 0.8$. It is then followed by a wobbling motion for $0.9 \leqslant Ca \leqslant 1.7$ and by an oscillating-swinging motion with decreasing oscillation about the shear plane as $Ca$ increases (Figure 15).

In conclusion we find the same qualitative motion (rolling followed by wobbling and

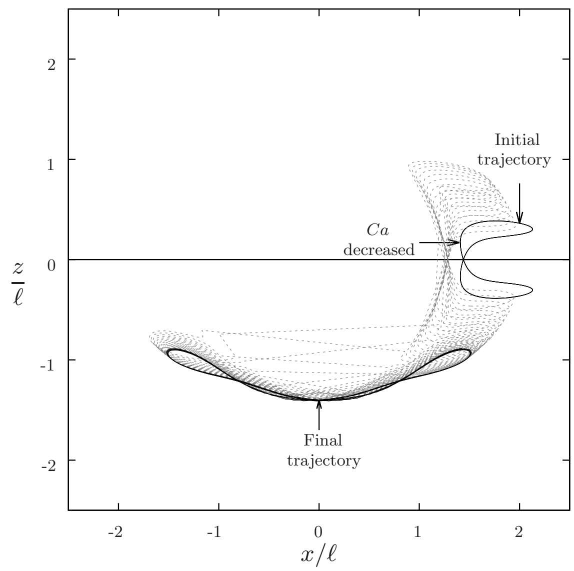


Figure 13: Time evolution of a capsule C2SK initially undergoing stable oscillating-swinging motion at $Ca = 1.5$, when the capillary number is suddenly changed to $Ca = 0.9$. The trajectory of the capsule tip P" in the $xz-$plane is followed in time.

eventually swinging with oscillations about the shear plane), irrespective of the capsule membrane law or aspect ratio. The main effect of these parameters is to change a little the values of $Ca$ at transition. In particular, it seems that the main factor that triggers the transition from rolling to wobbling is the deformation of the membrane. Indeed, from Figure 14, we note that the last result of stable rolling motion before transition is obtained for roughly the same values of the three deformation parameters

$$D_{23} = 0.45 \sim 0.47, \quad |D_{12} - D(0)_{12}| = 0.23, \quad D_{13} - D(0)_{13} = 0.16 \sim 0.22,$$

where $D(0)_{ij}$ is the initial capsule apparent deformation due to the anisotropic ellipsoidal shape. This means that it corresponds to the same mean elastic energy in the membrane $E/G_s\ell^2 = 1 \sim 1.3$, which is rather small compared to the high levels of elastic energy reached in the swinging regime.

## 5. Discussion and conclusion

The study of the mechanical stability of the motion of a prolate ellipsoidal capsule under shear flow has provided new interesting results. We have found that for a prolate capsule in Stokes flow, the two obvious symmetric configurations where the capsule axis is either parallel or perpendicular to the shear plane do not always correspond to stable equilibrium states. Since in the Stokes regime, the dynamic time dependent term is removed from the Navier–Stokes equations, the only way to test the stability of an equilibrium solution is to perturb it. We have adopted this method and showed that for low flow strength, the capsule will assume a rolling motion with its axis parallel to the flow vorticity, whereas for high flow strength, the swinging motion in the shear plane is stable. We have not tried to determine with a high precision, the values of $Ca$ for which transition occurs. The critical value is obtained within an interval of 0.1.

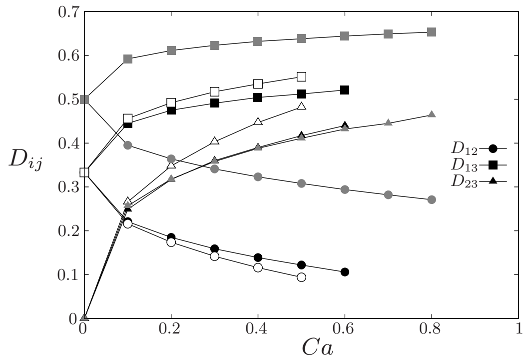


Figure 14: Influence of the capillary number $Ca$ on the capsule deformation estimated by the Taylor parameters $D_{ij}$ during the stable rolling regime $\zeta_0 = 0°$. Open symbols: C2NH; black closed symbols: C2SK; grey closed symbols: C3SK.

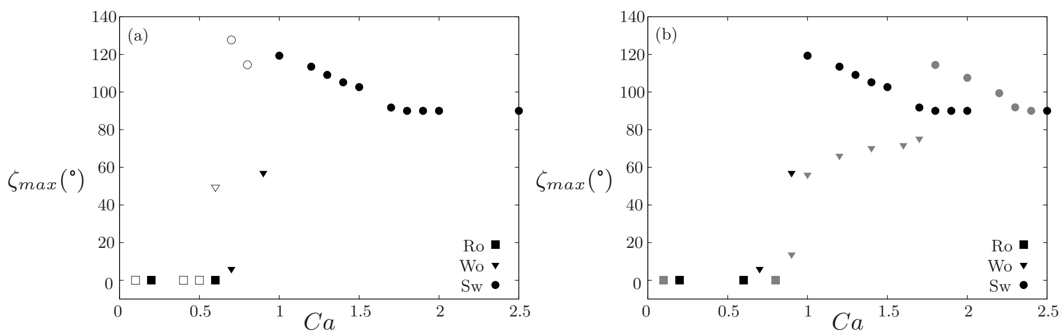


Figure 15: Influence of the constitutive law (a) and of the aspect ratio (b) on the maximum inclination $\zeta_{max}$ as a function of $Ca$. Ro: rolling; Wo: wobbling; Sw: oscillating-swinging tending to pure swinging; open symbols: C2NH; black closed symbols: C2SK; grey closed symbols: C3SK.

For example, in the case of a capsule with $a/b = 2$ and a SK ($C = 1$) membrane, we find that for moderate flow strength (up to $Ca = 0.6$), the stable equilibrium corresponds to the rolling regime: the prolate capsule orients its long axis parallel to the vorticity direction. For high flow strength ($Ca \geqslant 1.8$), the capsule, however, places its long axis in the shear plane and follows a swinging regime with oscillations decreasing with $Ca$. In the intermediate range ($0.7 \leqslant Ca \leqslant 0.9$), the capsule first exhibits a complex wobbling motion and precesses around the vorticity axis. Its long axis then makes a mean angle with the vorticity axis which increases with $Ca$. For $Ca > 1$, the capsule oscillates about the shear plane and assumes a swinging motion. The amplitude of the oscillations decrease with $Ca$.

Jeffery (1922) found that the final orientation of a rigid ellipsoidal particle suspended in an external flow was such that the viscous energy dissipation is minimum. Correspondingly, a prolate ellipsoid would have its long axis parallel to the vorticity. For small capillary numbers, the capsule behaves almost like a solid ellipsoid. It is thus not surprising that the stable equilibrium state, i.e. the rolling regime, corresponds to the Jeffery's regime. For $Ca > 0.6$, the capsule no longer converges towards the configuration that minimizes the viscous dissipation as can be surmised from Figures 8 and 11. The membrane deformation plays an important role and the fluid-structure interactions dictate the equilibrium configuration. We have corroborated these results by studying other prolate capsules with either a different membrane law or a different aspect ratio. We find that all these capsules have a stable rolling regime at low shear rate, from which they depart when a given level of deformation (or of elastic energy in the membrane) is reached. This allows us to surmise the role of the viscosity ratio $\eta$ between the internal and external fluids. Using a viscosity ratio $\eta = 1$ simplifies significantly the computations which are then shorter. As we have studied the dynamic response of a capsule this is an appreciable advantage. For spherical capsules, it has been shown that $\eta < 1$ leads to a moderate increase of the capsule deformation of order 20% for the same value of $Ca$ (Foessel *et al.* 2011). Thus we can expect a low internal viscosity capsule to quit the rolling regime for values of $Ca$ lower than those found for $\eta = 1$. Conversely as $\eta$ increases above unity, the internal viscosity effect is to decrease the capsule deformability. We can thus expect that the stability limit of the rolling regime will increase with the internal viscosity.

Experimentally, for a given capsule population, the capsule shape (size ratio $a/b$ and characteristic length $\ell$), internal viscosity $\mu$ and membrane elasticity moduli ($G_s$, $K_s$) are fixed. Thus the only way to increase $Ca$ is through the shear rate $\dot{\gamma}$ and the external fluid viscosity (but then the viscosity ratio also changes while it is assumed to be unity in this study). Typical artificial capsules have a shear elastic modulus of the order of $G_s = 0.1$ to 1 N/m (Chang & Olbricht 1993; Chu *et al.* 2011; Koleva & Rehage 2012; Zhang & Salsac 2012), while their size varies from $\ell = 30$ $\mu$m to 1 mm. With these values, we have to apply a viscous stress $\mu\dot{\gamma}$ of the order of 100 Pa to obtain a capillary number of $Ca = 0.1$. At the same time, we have to keep the flow Reynolds number $Re = \rho a^2 \dot{\gamma}/\mu$ small (where $\rho$ is the fluid density). Experimental observations are best made at low values of the shear rate, typically $\dot{\gamma} < 10$ s$^{-1}$ so that the experimental time $t$ is not too short (see for example Abkarian *et al.* (2007)). Thus high values of the shear stress are difficult to achieve unless the external fluid viscosity is very large. We conclude that it is challenging to reach large values of $Ca$ experimentally.

Furthermore, artificial capsules tend to break up for deformation levels of order 2-10% (Chang & Olbricht 1993; Koleva & Rehage 2012) with a polymer membrane and of order 20-30% for a polymerized albumin membrane (Carin *et al.* 2003). It follows that although interesting from the theoretical point of view, the high $Ca$ behavior is not very likely to be observed. Thus, the most probable configuration that can be observed experimentally is the rolling regime.

**Acknowledgments**

This research is funded by the Conseil Régional de Picardie (MODCAP grant), by the French Ministère de la Recherche (Pilcam2 grant) and by the French Agence Nationale de la Recherche (CAPSHYDR grant ANR-11-BS09-013).

## REFERENCES

Abkarian, M., Faivre, M. & Viallat, A. 2007 Swinging of red blood cells under shear flow. *Physical Review Letters* **98**, 188302.

Abkarian, M., Lartigue, C. & Viallat, A. 2001 Motion of phospholipidic vesicles along an inclined plane: sliding and rolling. *Physical Review E* **63**, 041906.

Abkarian, M. & Viallat, A. 2008 Vesicles and red blood cells in shear flow. *Soft Matter* **4**, 653–657.

Andry, M.-C., Edwards-Lévy, F. & Lévy, M.-C. 1996 Free amino group content of serum albumin microcapsules. III. A study at low pH values. *International Journal of Pharmaceutics* **128** (12), 197 – 202.

Barthès-Biesel, D. 2011 Modeling the motion of capsules in flow. *Current Opinion in Colloid and Interface Science* **16**, 3–12.

Barthès-Biesel, D., Diaz, A. & Dhenin, E. 2002 Effect of constitutive laws for two-dimensional membranes on flow-induced capsule deformation. *Journal of Fluid Mechanics* **460**, 211–222.

Barthès-Biesel, D. & Rallison, J. M. 1981 The time-dependent deformation of a capsule freely suspended in a linear shear flow. *Journal of Fluid Mechanics* **113**, 251–267.

Barthès-Biesel, D., Walter, J. & Salsac, A.-V. 2010 *Computational hydrodynamics of capsules and biological cells*, chap. Flow-induced deformation of artificial capsules, pp. 35–70. Taylor & Francis.

Carin, M., Barths-Biesel, D., Edwards-Lvy, F., Postel, C. & Andrei, D. C. 2003 Compression of biocompatible liquid-filled HSA-alginate capsules: Determination of the membrane mechanical properties. *Biotechnology and Bioengieering* **82**, 207 – 212.

Chang, K. S. & Olbricht, W.L. 1993 Experimental studies of the deformation and breakup of a synthetic capsule in steady and unsteady simple shear flow. *Journal of Fluid Mechanics* **250**, 609–633.

Chang, T.M.S., Macintosh, F.C. & Mason, S.G. 1966 Semipermeable aqueous microcapsules: I. Preparation and properties. *Canadian Journal of Physiology and Pharmacology* **44**, 115–128.

Chu, T.X., Salsac, A.-V., Leclerc, E., Barthès-Biesel, D., Wurtz, H. & Edwards-Lvy, F. 2011 Comparison between measurements of elasticity and free amino group content of ovalbumin microcapsule membranes: Discrimination of the cross-linking degree. *Journal of Colloid and Interface Science* **355** (1), 81 – 88.

Dupire, J., Socol, M. & Viallat, A. 2012 Full dynamics of a red blood cell in shear flow. *Proceedings of the National Academy of Sciences* **109 (51)**, 20808 – 13.

Edwards-Lévy, F., Andry, M.-C. & Lévy, M.-C. 1993 Determination of free amino group content of serum albumin microcapsules using trinitrobenzenesulfonic acid: effect of variations in polycondensation pH. *International Journal of Pharmaceutics* **96** (13), 85 – 90.

Edwards-Lévy, F., Andry, M.-C. & Lévy, M.-C. 1994 Determination of free amino group content of serum albumin microcapsules: II. effect of variations in reaction time and in terephthaloyl chloride concentration. *International Journal of Pharmaceutics* **103** (3), 253 – 257.

Foessel, E., Walter, J., Salsac, A.-V. & Barthès-Biesel, D. 2011 Influence of internal viscosity on the large deformation and buckling of a spherical capsule in a simple shear flow. *Journal of Fluid Mechanics* **672**, 477–486.

Hay, K. L. & Bull, B. S. 2009 Statistical clues to postoperative blood loss: Moving averages applied to medical data. *Blood Cells, Molecules, and Diseases* **43** (3), 250 – 255.

Jeffery, G. B. 1922 The motion of ellipsoidal particles immersed in a viscous fluid. *Proceedings of the Royal Society A* **102**, 161–179.

Koleva, I. & Rehage, H. 2012 Deformation and orientation dynamics of polysiloxane microcapsules in linear shear flow. *Soft Matter* **8**, 3681–3693.

Lac, E., Barthès-Biesel, D., Pelakasis, A. & Tsamopoulos, J. 2004 Spherical capsules in three-dimensional unbounded Stokes flows: effect of the membrane constitutive law and onset of buckling. *Journal of Fluid Mechanics* **516**, 303–334.

Lévy, M.-C., Andry, M.-C., Lefebvre, S. & Manfait, M. 1995 Fourier transform infrared spectroscopic studies of cross-linked human serum albumin microcapsules. 3. influence of terephthaloyl chloride concentration on spectra and correlation with microcapsule morphology and size. *Journal of Pharmaceutical Sciences* **84** (2), 161–165.

Lévy, M.-C., Lefebvre, S., Andry, M.-C., Rahmouni, M. & Manfait, M. 1994 Fourier-transform infrared spectroscopic studies of cross-linked human serum albumin microcapsules. 2. Influence of reaction time on spectra and correlation with microcapsule morphology and size. *Journal of Pharmaceutical Sciences* **83** (3), 419–422.

Lévy, M.-C., Lefebvre, S., Rahmouni, M., Andry, M.-C. & Manfait, M. 1991 Fourier transform infrared spectroscopic studies of human serum albumin microcapsules prepared by interfacial cross-linking with terephthaloylchloride: Influence of polycondensation pH on spectra and relation with microcapsule morphology and size. *Journal of Pharmaceutical Sciences* **80** (6), 578–585.

Li, X. & Sarkar, K. 2008 Front tracking simulation of deformation and buckling instability of a liquid capsule enclosed by an elastic membrane. *Journal of Computational Physics* **227**, 4998–5018.

Liu, L., Yang, J.-P, Ju, X.-J., Xie, R., Yang, L., Liang, B. & Chu, L.-Y. 2009 Microfluidic preparation of monodisperse ethyl cellulose hollow microcapsules with non-toxic solvent. *Journal of Colloid and Interface Science* **336 (1)**, 100–106.

Ramanujan, S. & Pozrikidis, C. 1998 Deformation of liquid capsules enclosed by elastic membranes in simple shear flow: Large deformations and the effect of capsule viscosity. *Journal of Fluid Mechanics* **361**, 117–143.

Schneeweiss, I. & Rehage, H. 2005 Non-spherical capsules for the food industry. *Chemie Ingenieur Technik* **77 (3)**, 236–239.

Skalak, R., Tozeren, A., Zarda, R. P. & Chien, S. 1973 Strain energy function of red blood cell membranes. *Biophysical Journal* **13**, 245–264.

Sui, Y., Low, H. T., Chew, Y. T. & Roy, P. 2008 Tank-treading, swinging, and tumbling of liquid-filled elastic capsules in shear flow. *Physical Review E* **77**, 016310.

Walter, A., Rehage, H. & Leonhard, H. 2001 Shear induced deformation of microcapsules: shape oscillations and membrane folding. *Colloids and Surfaces A: Physicochemical and Engineering Aspects* **183-185**, 123–132.

Walter, J., Salsac, A.-V. & Barthès-Biesel, D. 2011 Ellipsoidal capsules in simple shear flow: prolate versus oblate initial shapes. *Journal of Fluid Mechanics* **676**, 318–347.

Walter, J., Salsac, A.-V., Barthès-Biesel, D. & Le Tallec, P. 2010 Coupling of finite element and boundary integral methods for a capsule in a Stokes flow. *International Journal for Numerical Methods in Engineering* **83**, 829–850.

Xiang, Z. Y., Lu, Y. C., Zou, Y., Gong, X. C. & Luo, G. S. 2008 Preparation of microcapsules containing ionic liquids with a new solvent extraction system. *Reactive and Functional Polymers* **68 (8)**, 1260–1265.

Zhang, L. & Salsac, A.-V. 2012 Can sonication enhance release from liquid-core capsules with a hydrogel membrane? *Journal of Colloid and Interface Science* **368**, 648–654.